Preparation of NaYF$_4$:Yb,Tm/TiO$_2$/RGO composite and photocatalytic degradation of nitenpyram

Mingyue Piao[a,b], Huishi Du[c], Yuwei Sun[a,b], Yixuan Wang[b], Honghui Teng[a,b,*]

[a]*Key Laboratory of Environmental Materials and Pollution Control, the Education Department of Jilin Province, Jilin Normal University, Siping, China, email: tenghh888@163.com (H.H. Teng)*
[b]*College of Engineering, Jilin Normal University, Siping, China*
[c]*College of Tourism and Geographical Science, Jilin Normal University, Siping, China*

ABSTRACT

A ternary photocatalytic composite NaYF$_4$:Yb,Tm/TiO$_2$/RGO was synthesized by hydrothermal method, and it was characterized by scanning electron microscopy, X-ray diffraction, UV-Vis diffuse reflectance spectroscopy, Fourier-transform infrared spectroscopy and photoluminescence spectroscopy. The effect of pH, dosage of catalyst, and initial concentration of nitenpyram on degradation efficiency were tested. The best results were occurred on pH 9, and dosage 1.0 g/L. Higher concentration of nitenpyram was not favorable for photocatalysis due to the inhibition of UV penetration. The obtained ternary composite exhibited a significant enhancement in photocatalytic efficiency, and about 76.08% of nitenpyram was degraded within 60 min under UV irradiation. Furthermore, NaYF$_4$:Yb,Tm/TiO$_2$/RGO can be reused for 6 times without significant catalysis loss. During nitenpyram photocatalytic degradation, photo-induced holes and hydroxyl radicals may be the two main active species according to trapping experiments. The possible intermediate product was put forwarded.

Keywords: Intermediate product; NaYF$_4$:Yb,Tm/TiO$_2$/RGO; Nitenpyram insecticide; Photocatalysis; Reuse; Trapping experiment

1. Introduction

China is one of the largest agricultural countries, and it consumes plenty of pesticides in the world. Pesticides usually are not absorbed by weeds and pests fully, thus this widely use of them has lead to high level of residues in the environment. Nitenpyram has been extensively used in agricultural industry by virtue of its high insecticidal activity, wide spectrum, low toxic and low residue. More importantly, it acts selectively on the insect central nervous system [1]. However, the widely use of nitenpyram may contribute to the declined biodiversity of non-target terrestrial insects [2], and takes a risk to soil ecosystems [3] and human health [4]. In addition, there is a high possibility of it entering aquatic ecosystems through runoff, and thus potentially may pose threat to aquatic organisms [5,6]. Nitenpyram has been detected in some surface rivers in China [7–10], Spain [11], India [12], USA [13] and UK [14], so it is necessary to remove them from aqueous environment.

Many works have confirmed that adsorption [15], advanced oxidation processes [16] and microbial biodegradation [17], can be effectively used for nitenpyram removal. Compared with those methods, photocatalysis has intrigued much attention due to its environmental benignity and high-efficiency [18–20]. Ag@AgCl [21], Ag$_3$PO$_4$ [22], g-C$_3$N$_4$ [23], BiVO$_4$ [24], and other photo catalysts have efficient function on nitenpyram elimination. Up conversion nanoparticles (UCNPs) are an interesting class that have been currently investigated due to their concerted recombination of dual or multi lower-energy photons, resulting

* Corresponding author.

in the luminescence of higher-energy (lower wavelength) photons. However, the inherently low UC emission efficiency of the newly synthesized UCNPs is a major challenge for their direct practical use. The above-mentioned defect can be solved by doping UCNPs with metal ion or metallic oxide. Ren et al found that $NaYF_4$:Yb,Tm combined with Ce^{3+} ions could promote the efficient energy transfer between core-shell structure [25]. Photocatalytic hydrogen evolution would be promoted by synergistic effect between $NaYF_4$:Yb,Er and CdS composites [26]. TiO_2 is a kind of widely used photocatalyst to degrade organic pollutants, due to its good stability and low price [27–29]. Reduced graphene oxide (RGO) also attracts immense attention due to its high activity and large surface area with excellent electron mobility and thermal stability, thus always acts as electron acceptor in photocatalytic reactions to increase the separation rate of photo-generated electrons and holes [30]. It has been already proven that by introducing RGO into TiO_2 can effectively promote the transfer of photo-induced electron–hole pairs to generate more hydroxyl radicals and superoxide anions [31].

In this work, a ternary composite $NaYF_4$:Yb,Tm/TiO_2/RGO was fabricated via hydrothermal method, and further used for nitenpyram removal. The as-prepared photocatalyst showed a good photo stability during recycling experiments. Based on experimental results, the main active species was confirmed.

2. Materials and methods

2.1. Chemicals and materials

Graphite, Y_2O_3, Tm_2O_3, Yb_2O_3, NH_4F, polyvinylpyrrolidone (PVP), TBOT and anhydrous ethanol were purchased from Sinopharm Chemical Reagent Co., Ltd., (Shanghai, China). All the reagents were used without further purification. Deionized water (DW) was used throughout this work.

2.2. Synthesis of $NaYF_4$:Yb,Tm/TiO_2/RGO

$NaYF_4$:Yb,Tm and graphene oxide (GO) were prepared following the Huangs' [32] and the modified Hummers' method [33]. TBOT (8.5 mL) was dissolved in 50 mL of ethanol and stirred for 30 min, then 5 mL of DW dropped into it. $NaYF_4$:Yb,Tm (0.05 g) and 0.012 g of GO were added into the solution. Until blending thoroughly, the mixture was transferred to a 100 mL of Teflon reactor, followed by reacting at 180°C for 12 h. The solution was washed with anhydrous ethanol and centrifuged, and the obtained precipitate was washed with DW for 3 times. The synthesized products was labeled as $NaYF_4$:Yb,Tm/TiO_2/RGO.

2.3. Characterization of $NaYF_4$:Yb,Tm/TiO_2/RGO

The catalyst was coated with gold to form a thin layer, and imaged by scanning electron microscopy (SEM; JSM-7800F, Prime, Japan) under vacuum at 15 kV. The crystalline structure was detected by X-ray diffraction (XRD; D/max 2500, Rigaku, Japan) in a range of $2\theta = 5°\sim90°$ with Cu Kα radiation ($\lambda = 1.5406$ Å, 40 kV, 200 mA). UV-Vis spectrum was tested by UV-Vis spectrophotometer (UV-3600, Shimadzu, Japan). The photoluminescence property (PL)

was operated by the photoluminescence detector (F4500, Hitachi, Japan) with an excitation wavelength at 525 nm. Fourier-transform infrared spectroscopy (FTIR) spectrum was detected (Cary 660, Agilent, USA) after grinding the sample into powder and mixing well with KBr.

2.4. Photodegradation and its mechanism

The degradation efficiency of nitenpyram was used to evaluate the photocatalytic performance of the prepared composites. The simulated UV irradiation was achieved by a UV lamp (40 W). Specially, 50 mg of photocatalyst was added into nitenpyram solution ($V = 50$ mL, $C_{nitenpyram} = 50$ mg/L, pH = 9) with continuous stirring for 30 min. Before light irradiation, the solution was stirred in a darkroom for 30 min to reach adsorption equilibrium. The concentration of nitenpyram was tested by UV spectrophotometry at 269 nm.

3. Results and discussions

3.1. Characterization of $NaYF_4$:Yb,Tm/TiO_2/RGO

Fig. 1a shows that $NaYF_4$:Yb,Tm was spherical with a particle size of about 50 nm, while TiO_2 was also spherical with a particle size of about 100 nm (Fig. 1b). When $NaYF_4$:Yb,Tm and TiO_2 loaded in RGO (Fig. 1c), the ternary composite showed plate structure due to RGO. Energy-dispersive X-ray spectroscopy (EDX) mapping proved that C, Ti, Yb, Y and Tm were presented in $NaYF_4$:Yb,Tm/TiO_2/RGO, indicating that all the raw materials were combined together.

Fig. 2a shows that XRD pattern of TiO_2 exhibited a strong diffraction peak around $2\theta = 25.2°$, $38.0°$, $48.1°$, $54.1°$, $62.7°$ and $71.7°$, corresponding to crystalline phases of (101), (004), (200), (105), (204) and (220), respectively, which was in good according with TiO_2 standard card well (JCPDS No. 65-2448). The ternary composite $NaYF_4$:Yb,Tm/TiO_2/RGO shows the similar pattern with TiO_2 due to smaller proportion of $NaYF_4$:Yb,Tm and RGO in the composite material. Fig. 2b shows various chemical bonds in ternary composite, much are similar with TiO_2. And some bands respective of $NaYF_4$:Yb,Tm also presented in ternary composite, such as F (1,385 cm^{-1}), indicating that $NaYF_4$:Yb,Tm was successfully doped in TiO_2. In Fig. 2c TiO_2 displays a strong absorption in UV regions, especially in 406.7 nm. After doping with $NaYF_4$:Yb,Tm, the absorption band edge was close to 387.5 nm, indicating that blue-shift was occurred, and composite material increased the intensity of spectral response. As we known, the fuorescence intensity of photocatalyst is positively correlated with the recombination rate of electrons and holes pairs. As shown in Fig. 2d, TiO_2 showed a strong peak at 1,052 nm, and it decreased significantly in the ternary composites, indicating that the faster charge separation efficiency.

3.2. Photocatalytic studies

3.2.1. Photocatalytic influence factors

Fig. 3a shows that pH had a significant impact on photocatalytic activity, and the photodegradation efficiency of
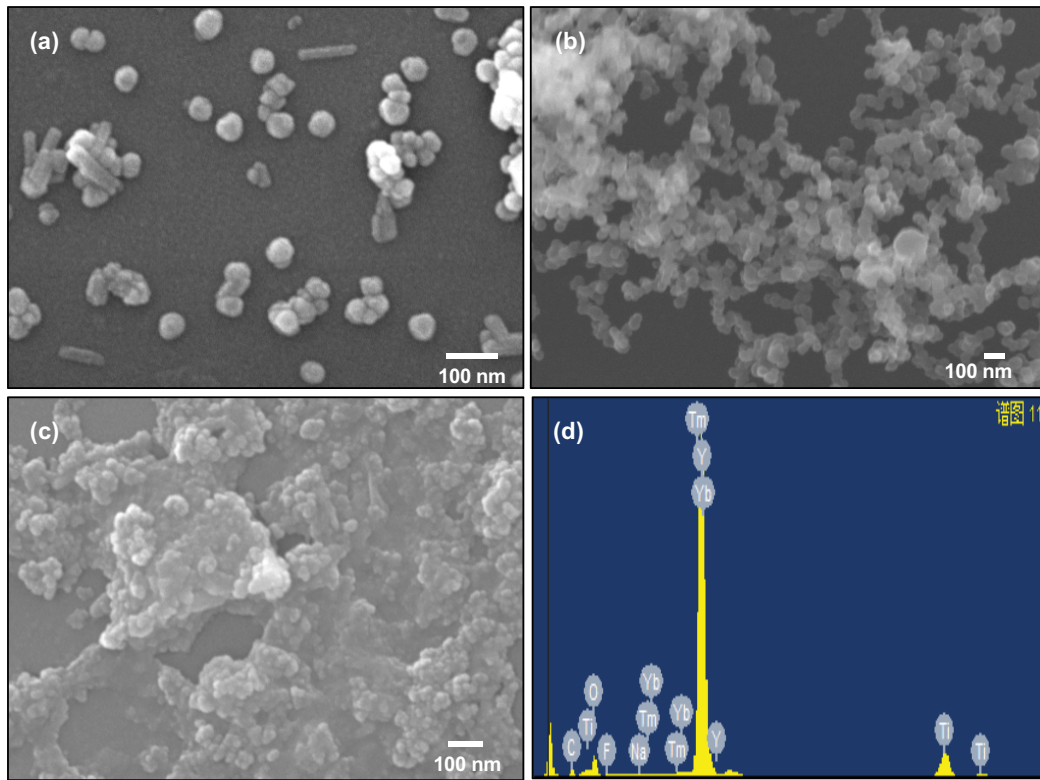
Fig. 1. SEM of (a) NaYF$_4$:Yb,Tm, (b) TiO$_2$, and (c) NaYF$_4$:Yb,Tm/TiO$_2$/RGO. (d) EDX mapping of NaYF$_4$:Yb,Tm/TiO$_2$/RGO.
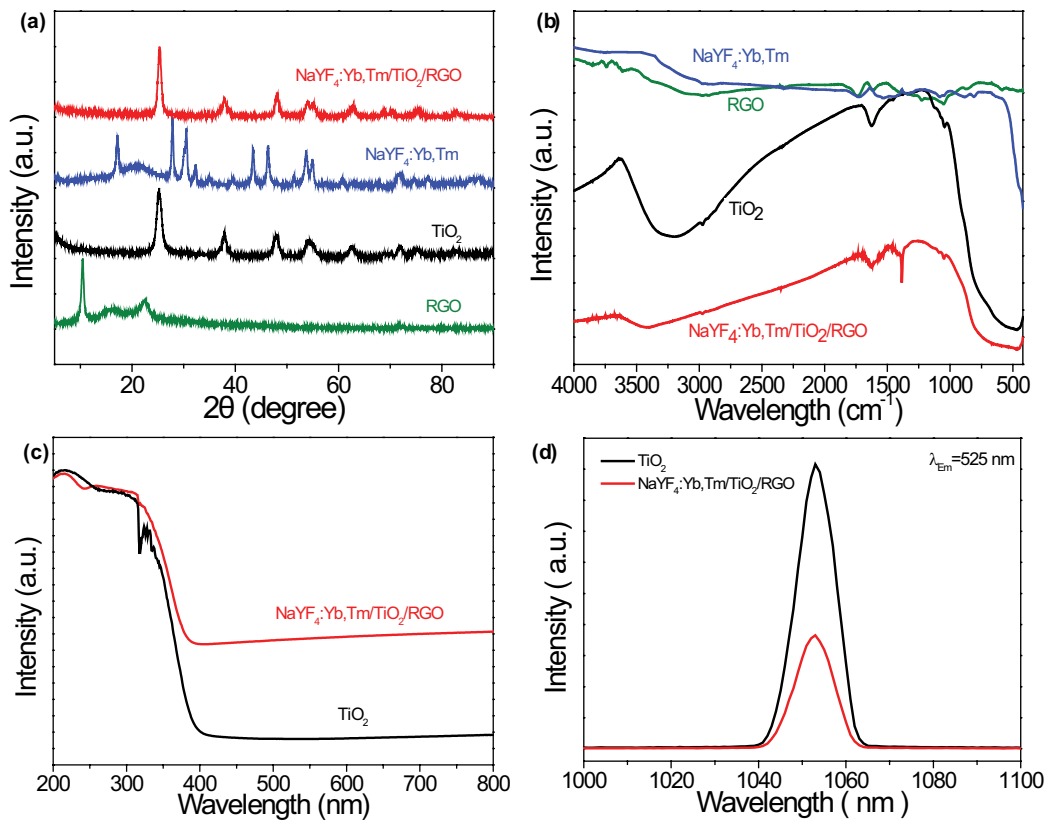
Fig. 2. (a) XRD pattern, (b) FTIR spectra, (c) UV-Vis diffuse reflectance spectra and (d) PL spectrum of the prepared composites.
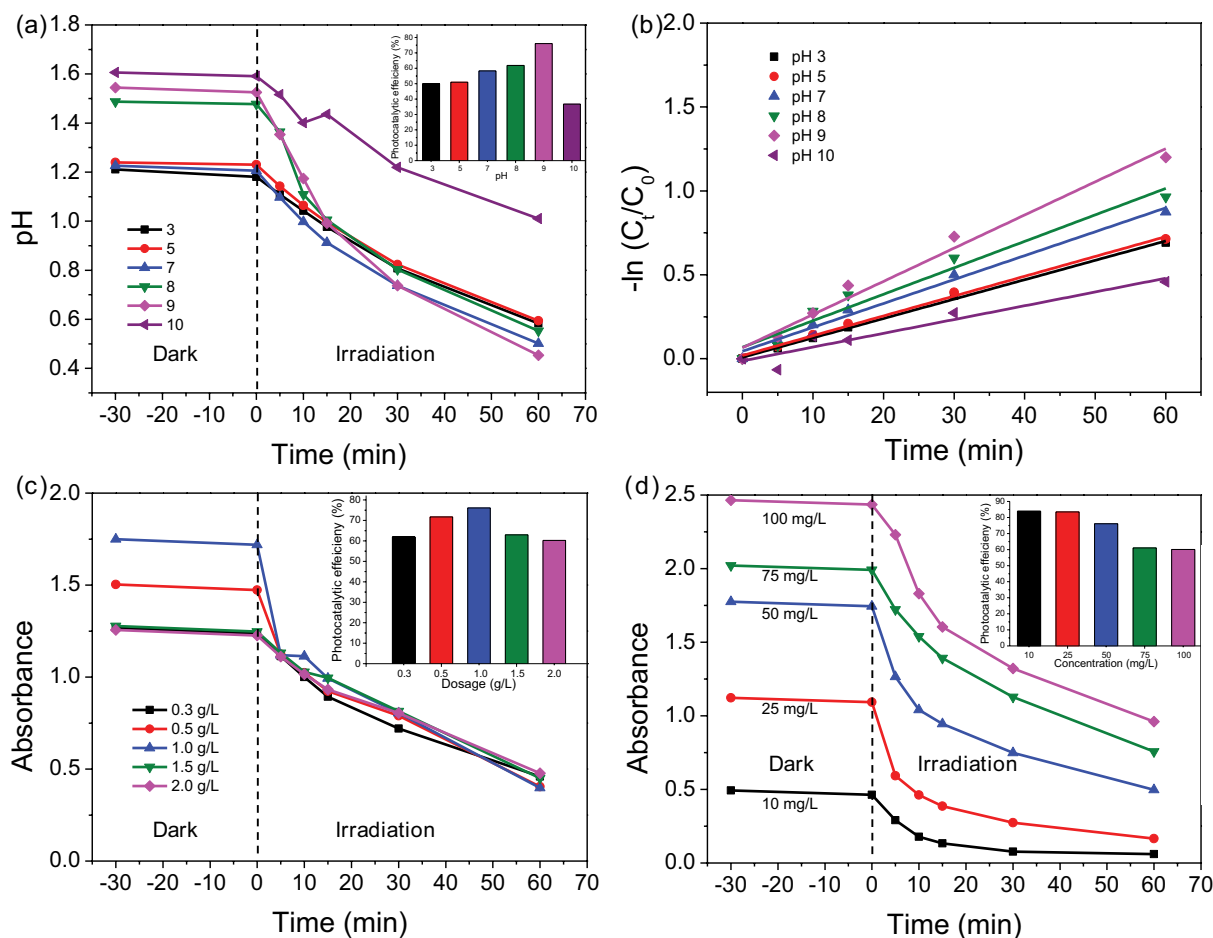
Fig. 3. Effect of (a) pH on photodegradation efficiency and (b) its degradation kinetics. Effect of (c) catalyst dosage and (d) initial concentration of nitenpyram on photodegradation efficiency.

nitenpyram was 49.90%, 50.98%, 58.30%, 61.83%, 76.08% and 36.70%, corresponding to pH 3.0, 5.0, 7.0, 8.0, 9.0 and 10.0, respectively. On the surface of the composite catalyst, a charge interference layer may be formed in acidic condition, which prevented the contact between nitenpyram and the catalyst, resulting in a decrease in the degradation efficiency. According to the fitting curve as shown in Fig. 3b, based on $-\ln(C_t/C_0)$ vs. t, the correlation coefficients (R^2) were all bigger than 0.9 showing that photocatalytic degradation of nitenpyram fitted well with first-order kinetic. The maximum rate constant was 0.024 which occurred at pH 9.0. Fig. 3c illustrates the influence of catalyst dosage on degradation efficiency. With the increase of catalyst amount, the removal efficiency increased first and then decreased. The best removal efficiency (76.08%) was obtained when the dosage was 1.0 g/L. This indicated that a small amount of catalyst would favorable for its dispersing in the pollutants system, whereas excessive catalyst was not conducive to light penetration, preventing UV light from entering the reaction system, and decreasing the photocatalytic efficiency. Fig. 3d shows the changes of removal efficiency vs. the initial concentration of nitenpyram, and the removal efficiencies were 83.88%, 83.46%, 76.08%, 61.20% and 60.10%, respectively, decreased significantly with the increase of the

initial concentration of nitenpyram. This can be explained that too many pesticide molecules in simulated wastewater prolonged the path of photons into the solution, resulting in the reduced photocatalytic efficiency. In addition, when the concentration of insecticide was increased, the intermediate products generated in the reaction would also accumulate, which would further compete ·OH with nitenpyram in the aqueous solution.

Other photocatalysts for degradation of nitenpyram were compared to this catalyst as given in Table 1, and NaYF$_4$:Yb,Tm/TiO$_2$/RGO showed average performance among these photocatalysts.

3.2.2. Reusability of NaYF$_4$:Yb,Tm/TiO$_2$/RGO

Reusability is an important factor for catalyst application. After one cycle, fresh nitenpyram solution was reacted with the same catalyst, and the cycle test was conducted 6 times. As shown in Fig. 4, the photocatalytic activity of NaYF$_4$:Yb,Tm/TiO$_2$/RGO towards nitenpyram was relatively stable after 6 times reuse, and the relative degradation efficiency was about 99% compared with the first experiment, indicating that the catalyst had favourable stability.

Table 1
Photocatalytic degradation efficiencies of nitenpyram by different photocatalysts

Photocatalyst	Nitenpyram concentration (mg/L)	Time (min)	Efficiency (%)	References
$WO_3/ZnIn_2S_4$	3	40	74.1	[34]
Bi_2WO_6/Ag_3PO_4/Zn-Al LDH	50	90	100	[35]
Ag/Ag_3PO_4/Zn-Al LDH	50	60	100	[36]
Ag@AgCl/ZnAl-LDH	40	45	100	[22]
$g-C_3N_4/WO_3$	—	30	68	[37]
$NaYF_4$:Yb,Tm/TiO_2/RGO	50	60	76.08	This work
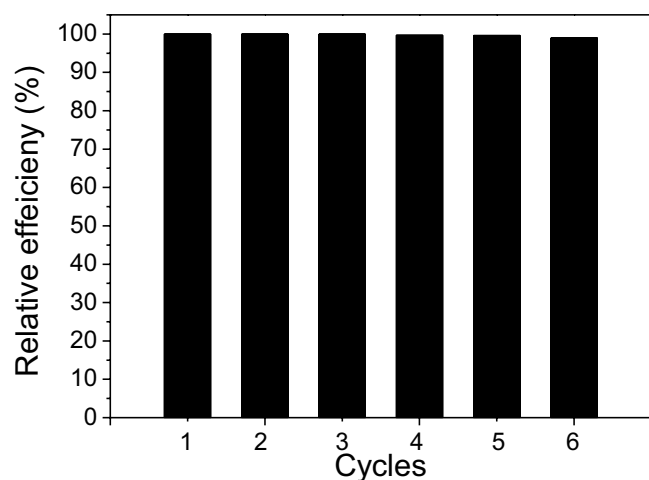
Fig. 4. Reusability of $NaYF_4$:Yb,Tm/TiO_2/RGO.
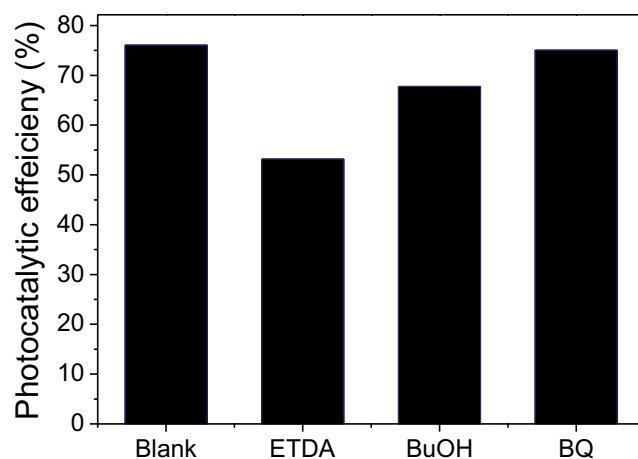
Fig. 5. Active species trapping experiments over $NaYF_4$:Yb,Tm/TiO_2/RGO.
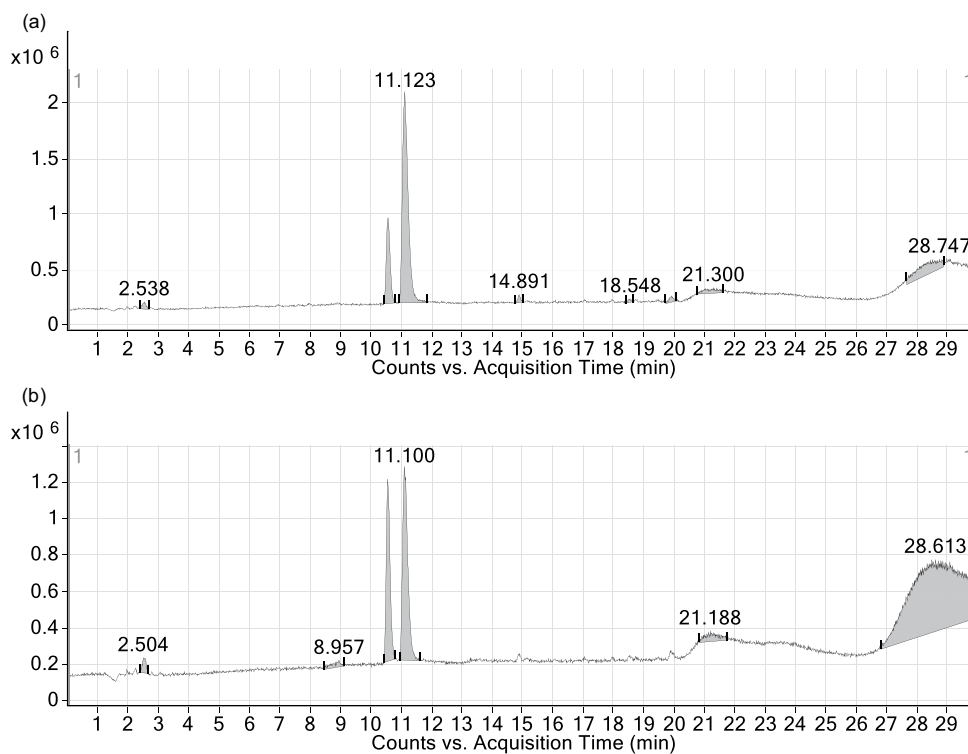
Fig. 6. Total ion flow diagram of HPLC when nitenpyram was degraded for (a) 60 min or (b) 120 min.
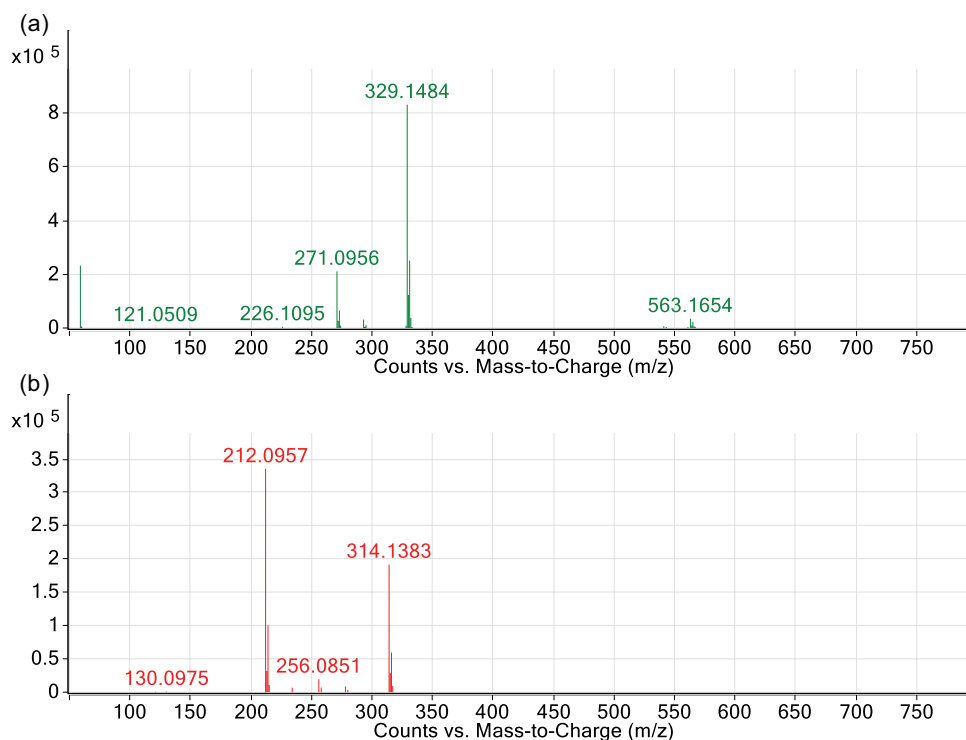
Fig. 7. Mass spectrum at retention time (a) 10.9~12.0 min and (b) 10.4~10.7 min of nitenpyram.

3.2.3. Trapping experiments

Different trapping agent was added during the catalytic process in order to investigate the photocatalytic oxidation mechanism. As shown in Fig. 5, the photodegradation of nitenpyram by $NaYF_4:Yb,Tm/TiO_2/RGO$ was not influenced by addition of 100 mg/L of BQ (a quencher of superoxide anion), but it decreased to 67.76% or 53.20% from 76.08% (blank) by adding 100 mg/L of BuOH (a quencher of hydroxyl radicals) or 100 mg/L of EDTA (a quencher of holes). In that case, we can concluded that photo-induced holes were the primary active species and hydroxyl radicals were the second active species in the nitenpyram photodegradation process by $NaYF_4:Yb,Tm/TiO_2/RGO$.

3.2.4. Possible pathway of nitenpyram degradation

Fig. 6 shows the total ion flow diagram of HPLC-MS when nitenpyram photodegraded by $NaYF_4:Yb,Tm/TiO_2/RGO$ after 60 min and 120 min. It can be seen that during the degradation process, nitenpyram (retention time at 10.9~12.0 min) was gradually degraded and products (retention time at 10.4~10.7 min) appeared. The integral area of the characteristic peak of nitenpyram decreased, and the characteristic peak of the product increased when the reaction time increased from 60 min to 120 min. The relative molecular weight of the main substances in the solution changed from 271 to 212 mol/z (Fig. 7). The pyridine ring in the molecular structure of nitenpyram was composed of five carbon atoms and one nitrogen atom. •OH first attacked the sites with high electron density in nitenpyram, and the N atoms on the ring fallen off to form NO^{2-} or NO^{3-}, and the remaining hydrogen atoms and N atoms were combined with the C atoms on both sides. Moreover, the C–Cl bond in the nitenpyram molecule was easy to break off due to the difference in the relative atomic mass between atoms, and the produced intermediate may be $C_{10}H_{18}N_3O_2$ (M = 212). Finally, nitenpyram molecules were disappeared and transferred to carbon and nitrogen-containing inorganic substances.

4. Conclusions

The photocatalyst $NaYF_4:Yb,Tm/TiO_2/RGO$ was prepared by hydrothermal process. The photocatalytic process was affected by pH of solution, dosage of catalyst and initial concentration of nitenpyram. Cycle experiments revealed a prominent reusability of the composites, which give a way for practical application. Under UV illumination, about 73% of nitenpyram was degraded within 60 min by $NaYF_4:Yb,Tm/TiO_2/RGO$. In the photodegradation process, photo-induced holes and hydroxyl radicals may be the major active species. During nitenpyram degradation, intermediate product $C_{10}H_{18}N_3O_2$ may be produced.

Declarations

Ethics approval and consent to participate

Not applicable.

Consent for publication

Not applicable.

Availability of data and materials

Not applicable.

Competing interests

The authors declare that they have no known competing financial interests or personal relationships that could have appeared to influence the work reported in this paper.

Authors' contributions

Mingyue Piao (writing and funding acquisition), Huishi Du (supervision and funding acquisition), Yuwei Sun (investigation and editing), Yixuan Wang (experiment performance), Honghui Teng (supervision and funding acquisition).

References

[1] C.C. Wu, S.D. Pan, Y.P. Shan, J.J. Cui, Y. Ma, Residue status and risk assessment of neonicotinoids under real field conditions: based on a two-year survey of cotton fields throughout China, Environ. Technol. Innovation, 28 (2022) 102689, doi: 10.1016/j.eti.2022.102689.

[2] M.A.I. Ahmed, C.F.A. Vogel, G. Malafaia, Short exposure to nitenpyram pesticide induces effects on reproduction, development and metabolic gene expression profiles in *Drosophila melanogaster* (*Diptera: Drosophilidae*), Sci. Total Environ., 804 (2022) 150254, doi: 10.1016/j.scitotenv.2021.150254.

[3] C.C. Wu, Z.N. Wang, Y. Ma, J.Y. Luo, X.K. Gao, J. Ning, X.D. Mei, D.M. She, Influence of the neonicotinoid insecticide thiamethoxam on soil bacterial community composition and metabolic function, J. Hazard. Mater., 405 (2021) 124275, doi: 10.1016/j.jhazmat.2020.124275.

[4] W. Liu, Z.C. Li, X.Y. Cui, F. Luo, C.Y. Zhou, J.Y. Zhang, L.G. Xing, Genotoxicity, oxidative stress and transcriptomic effects of Nitenpyram on human bone marrow mesenchymal stem cells, Toxicol. Appl. Pharm., 446 (2022) 116065, doi: 10.1016/j.taap.2022.116065.

[5] S.M. Crayton, P.B. Wood, D.J. Brown, A.R. Millikin, T.J. McManus, T.J. Simpson, K.-M. Ku, Y.-L. Park, Bioaccumulation of the pesticide imidacloprid in stream organisms and sublethal effects on salamanders, Global Ecol. Conserv., 24 (2020) e01292, doi: 10.1016/j.gecco.2020.e01292.

[6] L.B. Merga, P.J. Van den Brink, Ecological effects of imidacloprid on a tropical freshwater ecosystem and subsequent recovery dynamics, Sci. Total Environ., 784 (2021) 147167, doi: 10.1016/j.scitotenv.2021.147167.

[7] Z.K. Liu, S. Cui, L.M. Zhang, Z.L. Zhang, R. Hough, Q. Fu, Y.-F. Li, L.H. An, M.Z. Huang, K.Y. Li, Y.X. Ke, F.X. Zhang, Occurrence, variations, and risk assessment of neonicotinoid insecticides in Harbin section of the Songhua River, northeast China, Environ. Sci. Ecotechnol., 8 (2021) 100128, doi: 10.1016/j.ese.2021.100128.

[8] H.D. Tan, H.J. Zhang, C.Y. Wu, C.M. Wang, Q.F. Li, Pesticides in surface waters of tropical river basins draining areas with rice–vegetable rotations in Hainan, China: occurrence, relation to environmental factors, and risk assessment, Environ. Pollut., 283 (2021) 117100, doi: 10.1016/j.envpol.2021.117100.

[9] J.J. Xiong, B.X. Tan, X. Ma, H.Z. Li, J. You, Tracing neonicotinoid insecticides and their transformation products from paddy field to receiving waters using polar organic chemical integrative samplers, J. Hazard. Mater., 413 (2021) 125421, doi: 10.1016/j.jhazmat.2021.125421.

[10] Y.P. Zhang, H.F. Zhang, J. Wang, Z.Y. Yu, H.Y. Li, M. Yang, Suspect and target screening of emerging pesticides and their transformation products in an urban river using LC-QTOF-MS, Sci. Total Environ., 790 (2021) 147978, doi: 10.1016/j.scitotenv.2021.147978.

[11] L. Bijlsma, E. Pitarch, F. Hernández, E. Fonseca, J.M. Marín, M. Ibáñez, T. Portolés, A. Rico, Ecological risk assessment of pesticides in the Mijares River (eastern Spain) impacted by citrus production using wide-scope screening and target quantitative analysis, J. Hazard. Mater., 412 (2021) 125277, doi: 10.1016/j.jhazmat.2021.125277.

[12] Z.U. Shah, S. Parveen, Pesticide residues in *Rita rita* and *Cyprinus carpio* from river Ganga, India, and assessment of human health risk, Toxicol. Rep., 8 (2021) 1638–1644.

[13] S.M. Stackpoole, M.E. Shoda, L. Medalie, W.W. Stone, Pesticides in US Rivers: regional differences in use, occurrence, and environmental toxicity, 2013 to 2017, Sci. Total Environ., 787 (2021) 147147, doi: 10.1016/j.scitotenv.2021.147147.

[14] A.C. Taylor, G.A. Mills, A. Gravell, M. Kerwick, G.R. Fones, Passive sampling with suspect screening of polar pesticides and multivariate analysis in river catchments: informing environmental risk assessments and designing future monitoring programmes, Sci. Total Environ., 797 (2021) 147519, doi: 10.1016/j.scitotenv.2021.147519.

[15] Q.Z. Zhou, W.Z. Wang, F.M. Liu, R. Chen, Removal of difenoconazole and nitenpyram by composite calcium alginate beads during apple juice clarification, Chemosphere, 286 (2022) 131813, doi: 10.1016/j.chemosphere.2021.131813.

[16] T. González, J.R. Dominguez, S. Correia, Neonicotinoids removal by associated binary, tertiary and quaternary advanced oxidation processes: synergistic effects, kinetics and mineralization, J. Environ. Manage., 261 (2020) 110156, doi: 10.1016/j.jenvman.2020.110156.

[17] A.W. Chen, W.J. Li, X.X. Zhang, C. Shang, S. Luo, R.Y. Cao, D.D. Jin, Biodegradation and detoxification of neonicotinoid insecticide thiamethoxam by white-rot fungus *Phanerochaete chrysosporium*, J. Hazard. Mater., 417 (2021) 126017, doi: 10.1016/j.jhazmat.2021.126017.

[18] I. González-Mariño, I. Rodríguez, L. Rojo, R. Cela, Photodegradation of nitenpyram under UV and solar radiation: kinetics, transformation products identification and toxicity prediction, Sci. Total Environ., 644 (2018) 995–1005.

[19] S. Dolatabadi, M. Fattahi, M. Nabati, Solid state dispersion and hydrothermal synthesis, characterization and evaluations of TiO_2/ZnO nanostructures for degradation of Rhodamine B, Desal. Water Treat., 231 (2021) 425–435.

[20] H.A. Patehkhor, M. Fattahi, M. Khosravi-Nikou, Synthesis and characterization of ternary chitosan-TiO_2-ZnO over graphene for photocatalytic degradation of tetracycline from pharmaceutical wastewater, Sci. Rep., 11 (2021) 24177, doi: 10.1038/s41598-021-03492-5.

[21] Y.-J. Lee, J.-K. Kang, S.-J. Park, C.-G. Lee, J.-K. Moon, P.J.J. Alvarez, Photocatalytic degradation of neonicotinoid insecticides using sulfate-doped Ag_3PO_4 with enhanced visible light activity, Chem. Eng. J., 402 (2020) 126183, doi: 10.1016/j.cej.2020.126183.

[22] J.F. Zheng, X. Tang, C.Z. Fan, Y.C. Deng, X.M. Li, Q. Yang, D.B. Wang, A. Duan, J. Luo, Z. Chen, B.W. Zhang, Facile synthesis of Ag@AgCl/ZnAl-LDH sesame balls nanocomposites with enhanced photocatalytic performance for the degradation of neonicotinoid pesticides, Chem. Eng. J., 446 (2022) 136485, doi: 10.1016/j.cej.2022.136485.

[23] X. Liu, C.S. Li, B.J. Zhang, M. Yuan, Y.Q. Ma, F.Y. Kong, A facile strategy for photocatalytic degradation of seven neonicotinoids over sulfur and oxygen co-doped carbon nitride, Chemosphere, 253 (2020) 126672, doi: 10.1016/j.chemosphere.2020.126672.

[24] X.T. Liu, S.N. Gu, Y.J. Zhao, G.W. Zhou, W.J. Li, $BiVO_4$, Bi_2WO_6 and Bi_2MoO_6 photocatalysis: a brief review, J. Mater. Sci. Technol., 56 (2020) 45–68.

[25] H.H. Ren, F.H. Huang, J.M. Jiang, L. Wang, J.L. Zhang, Development of photocatalyst based on $NaYF_4$: Yb, Tm@$NaYF_4$: Yb, Ce/NH_2-MIL-101 (Cr): doping Ce^{3+} ions to promote the efficient energy transfer between core and shell, Chem. Eng. J., 427 (2022) 132023, doi: 10.1016/j.cej.2021.132023.

[26] H.Z. Zhu, Y.Q. Yang, Y.Y. Kang, P. Niu, X.D. Kang, Z.Q. Yang, H.Q. Ye, G. Liu, Strong interface contact between $NaYF_4$:Yb,Er and CdS promoting photocatalytic hydrogen evolution of $NaYF_4$:Yb,Er/CdS composites, J. Mater. Sci. Technol., 102 (2022) 1–7.

[27] H.P. Li, B. Sun, T.T. Gao, H. Li, Y.Q. Ren, G.W. Zhou, Ti_3C_2 MXene co-catalyst assembled with mesoporous TiO_2 for boosting photocatalytic activity of methyl orange degradation and hydrogen production, Chin. J. Catal., 43 (2022) 461–471.

[28] Y.C. Lu, X.Y. Ou, W.G. Wang, J.J. Fan, K.L. Lv, Fabrication of TiO_2 nanofiber assembly from nanosheets (TiO_2-NFs-NSs) by electrospinning-hydrothermal method for improved photoreactivity, Chin. J. Catal., 41 (2020) 209–218.

[29] J. Wang, G.H. Wang, B. Cheng, J.G. Yu, J.J. Fan, Sulfur-doped g-C_3N_4/TiO_2 S-scheme heterojunction photocatalyst for Congo red photodegradation, Chin. J. Catal., 42 (2021) 56–68.

[30] H. Mahmoodi, M. Fattahi, M. Motevassel, Graphene oxide–chitosan hydrogel for adsorptive removal of diclofenac from aqueous solution: preparation, characterization, kinetic and thermodynamic modelling, RSC Adv., 11 (2021) 36289–36304.

[31] H.Y. Fan, G.Y. Yi, Z.T. Zhang, X.X. Zhang, P. Li, C.X. Zhang, L.J. Chen, Y.L. Zhang, Q. Sun, Binary TiO_2/RGO photocatalyst for enhanced degradation of phenol and its application in underground coal gasification wastewater treatment, Opt. Mater., 120 (2021) 111482, doi: 10.1016/j.optmat.2021.111482.

[32] H.N. Huang, H.L. Li, Z.Y. Wang, P. Wang, Z.K. Zheng, Y.Y. Liu, Y. Dai, Y.J. Li, B.B. Huang, Efficient near-infrared photocatalysts based on $NaYF_4$:Yb^{3+},Tm^{3+}@$NaYF_4$:Yb^{3+},Nd^{3+}@TiO_2 core@shell nanoparticles, Chem. Eng. J., 361 (2019) 1089–1097.

[33] D.C. Marcano, D.V. Kosynkin, J.M. Berlin, A. Sinitskii, Z.Z. Sun, A. Slesarev, L.B. Alemany, W. Lu, J.M. Tour, Improved synthesis of graphene oxide, ACS Nano, 4 (2010) 4806–4814.

[34] M.L. Tang, Y.H. Ao, P.F. Wang, C. Wang, All-solid-state Z-scheme WO_3 nanorod/$ZnIn_2S_4$ composite photocatalysts for the effective degradation of nitenpyram under visible light irradiation, J. Hazard. Mater., 387 (2020) 121713, doi: 10.1016/j.jhazmat.2019.121713.

[35] J.F. Zheng, Y.C. Deng, C.Z. Fan, X.M. Li, D.X. Gong, C.W. Li, Z.Y. Ye, Novel Zn-Al LDHs based S-scheme heterojunction with coral reef-like structure for photocatalytic activation of peroxymonosulfate towards nitenpyram decomposition, J. Environ. Chem. Eng., 10 (2022) 108188, doi: 10.1016/j.jece.2022.108188.

[36] J.F. Zheng, W.B. Li, R.D. Tang, S. Xiong, D.X. Gong, Y.C. Deng, Z.P. Zhou, L. Li, L. Su, L.H. Yang, Ultrafast photodegradation of nitenpyram by Ag/Ag_3PO_4/Zn–Al LDH composites activated by persulfate system: removal efficiency, degradation pathway and reaction mechanism, Chemosphere, 292 (2022) 133431, doi: 10.1016/j.chemosphere.2021.133431.

[37] S.Q. Zhou, Y. Wang, K. Zhou, D.Y. Ba, Y.H. Ao, P.F. Wang, *In-situ* construction of Z-scheme g-C_3N_4/WO_3 composite with enhanced visible-light responsive performance for nitenpyram degradation, Chin. Chem. Lett., 32 (2021) 2179–2182.